The helicity constraint in spherical shell dynamos

A. Brandenburg[1], **P. J. Käpylä**[1,2], **D. Mitra**[3], **D. Moss**[4], **R. Tavakol**[3]

[1] NORDITA, Roslagstullsbacken 23, SE-10691 Stockholm, Sweden
[2] Observatory, University of Helsinki, PO Box 14, FI-00014 University of Helsinki, Finland
[3] School of Mathematical Sciences, Queen Mary, University of London, Mile End Road, London E1 4NS, UK
[4] School of Mathematics, University of Manchester, Oxford Road, Manchester M13 9PL, U.K.

February 2, 2008

The motivation for considering distributed large scale dynamos in the solar context is reviewed in connection with the magnetic helicity constraint. Preliminary accounts of 3-dimensional direct numerical simulations (in spherical shell segments) and simulations of 2-dimensional mean field models (in spherical shells) are presented. Interesting similarities as well as some differences are noted.

1 The context of the solar dynamo

At the moment we do not really know the location of the solar dynamo. It is widely assumed that it is located at the bottom of the convection zone, or that at least its toroidal field resides mostly at the bottom. However, this may not be the case, and instead a major part of the toroidal field may reside in the bulk of the convection zone – possibly even as high up as the near-surface shear layer, corresponding to the outer $35\,\mathrm{Mm}$ of the Sun (Brandenburg 2005). In this introductory section we discuss certain problems and properties associated with this proposal.

A particularly exciting possibility is to associate the equatorward migration of sunspot activity with the negative radial shear in the near-surface shear layer. This, together with a positive α effect in the northern hemisphere, could, according to standard mean-field theory (Krause & Rädler 1980), give rise to equatorward migration of the mean field. An obvious problem associated with this proposal is the fact that the near-surface shear layer is rather thin, and so the resulting aspect ratio of the container would favour solutions with many toroidal flux belts in one hemisphere (Moss et al. 1990).

Another potential problem might be the fact that the local turnover time in the near-surface shear layer is rather short (1 day compared to 12 days in the lower part of the convection zone). This is sometimes thought to be a difficulty if one wants to explain cycle times many times longer than this. However, it may not be justified to draw such a conclusion based on conventional mean field theory that ignores the effects of magnetic helicity conservation. This is true not only for near-surface shear layer dynamos, but even for what is now usually referred to as the Babcock-Leighton dynamo (Dikpati & Charbonneau 1999), which is based on a nonlocal α effect (the field at the bottom of the convection zone affects the electromagnetic force at the surface); see Brandenburg & Käpylä (2007) for an explicit demonstration. Even mean-field effects other than those based on an α effect, e.g. the so-called shear–current effect of Rogachevskii & Kleeorin (2003), produce magnetic helicity in the mean field and tend to generate also magnetic helicity of suitable sign in the small scale field in order to quench the dynamo. The latter drives a magnetic α effect that affects the mean electromotive force in a way which quenches the shear–current effect even if there is no kinetic α effect in the usual sense (Brandenburg & Subramanian 2005).

Quite generally, when the magnetic Reynolds number is large, mean field dynamos are only able to operate on time scales faster than the resistive time provided the resulting small scale magnetic helicity is shed from the dynamo domain. That the Sun sheds significant amounts of magnetic helicity through active regions and coronal mass ejections is now well known (Démoulin et al. 2002). Thus, it seems that an important ingredient of any solar dynamo model should be a penetrable surface that allows magnetic helicity to escape from the dynamo domain. An important aim of future work is therefore to improve our understanding of dynamos that are controlled by magnetic helicity fluxes.

Considerable progress has recently been made by using direct simulations of the solar dynamo. The simulations of Brun et al. (2004) and Browning et al. (2006) suggest that dynamo action in the lower overshoot layer leads to cyclic reversals. However, there is at present no clear evidence for migratory behaviour. On the other hand, current mean field modelling assumes that the magnetic field propagates equatorward due to the meridional circulation that flows equatorward at the bottom of the convection zone (e.g. Dikpati & Charbonneau 1999). However, this approach only works by assuming that the *turbulent* magnetic Prandtl number is about 100, which is hard to understand, because both theory and simulations suggest that this value should be around unity (Yousef et al. 2003). More importantly, circulation–dominated models neglect the effects of small scale magnetic helicity that contributes to the quenching of dynamo

action. It is therefore useful to establish details of magnetic helicity conservation in spherical geometry. In the present work we consider both direct three-dimensional simulations and two-dimensional mean field models.

2 The magnetic helicity constraint

In order to make contact between what has been learnt from Cartesian and spherical systems it is important to start with simple cases. This means closed (perfectly conducting) boundaries and fully helical turbulence in homogeneous (or nearly homogeneous) domains. At the level of mean field theory, this means a spatially constant α effect.

Of course, real systems are not uniform and the α effect changes sign across the equator. Nevertheless, for testing and illustrative purposes it is useful to consider a uniform α effect in spherical geometry (Krause & Rädler 1980). If there is only the α effect and turbulent diffusivity, $\eta_{\rm t}$, in addition to microscopic diffusivity, η, the mean magnetic field, $\overline{\boldsymbol{B}}$, is governed by the equation

$$\frac{\partial\overline{\boldsymbol{B}}}{\partial t}=\boldsymbol{\nabla}\times\alpha\overline{\boldsymbol{B}}+\eta_{\rm T}\nabla^2\overline{\boldsymbol{B}}, \tag{1}$$

where $\eta_{\rm T}=\eta_{\rm t}+\eta$ is the total magnetic diffusivity. (Both α and $\eta_{\rm T}$ are in this section assumed to be constants.) In a Cartesian domain of size L the critical value of α for dynamo action (i.e. exponentially growing solutions) is

$$\alpha/\eta_{\rm T}>k_1\equiv 2\pi/L. \tag{2}$$

For a full sphere the critical value is related to the first zero of the lowest order spherical Bessel function, i.e.

$$\alpha/\eta_{\rm T}>k_{1,\rm eff}\equiv 4.49/R. \tag{3}$$

In the present paper we are particularly interested in perfectly conducting boundary conditions, because in that case the magnetic helicity is conserved. This fact yields an interesting quantitative connection between the magnetic energies contained in large scale and small scale fields, as will be explained in the following. In a closed domain whose boundaries are not crossed by any field lines the evolution equation of magnetic helicity is given by

$$\frac{\rm d}{{\rm d}t}\int\boldsymbol{A}\cdot\boldsymbol{B}\,{\rm d}V=-2\eta\int\boldsymbol{J}\cdot\boldsymbol{B}\,{\rm d}V, \tag{4}$$

where $\boldsymbol{J}=\boldsymbol{\nabla}\times\boldsymbol{B}$ is the current density (in units where the permeability is unity) and $\boldsymbol{B}=\boldsymbol{\nabla}\times\boldsymbol{A}$ is the magnetic field expressed as the curl of the magnetic vector potential. The integral on the rhs of Eq. (4) is referred to as the current helicity. Remarkably, in the steady state we then have

$$\int\boldsymbol{J}\cdot\boldsymbol{B}\,{\rm d}V=0, \tag{5}$$

even though there can be strong driving of current helicity due to the helical nature of the forcing.

Such forcing produces primarily helical fields at the scale of the driving (we call the associated wavenumber $k_{\rm f}$). If this scale is small compared with the system size (associated wavenumber k_1), we can have current helicity of finite magnitude at small and large scales.

To elaborate on this further, we define mean fields by averaging over one or two coordinate directions and denote the result by an overbar, i.e. we have $\overline{\boldsymbol{J}}=\boldsymbol{\nabla}\times\overline{\boldsymbol{B}}$ and $\overline{\boldsymbol{B}}=\boldsymbol{\nabla}\times\overline{\boldsymbol{A}}$. The corresponding fluctuating fields are indicated by lower case symbols, i.e. $\boldsymbol{b}=\boldsymbol{B}-\overline{\boldsymbol{B}}$, etc., so the idea is then that

$$\langle\overline{\boldsymbol{J}}\cdot\overline{\boldsymbol{B}}\rangle=-\langle\boldsymbol{j}\cdot\boldsymbol{b}\rangle\neq 0, \tag{6}$$

where angular brackets indicate volume averages. The wave numbers (inverse length scales) associated with large and small scale fields, $k_{\rm m}$ and $k_{\rm f}$, respectively, can be given as

$$k_{\rm m}^2\equiv\langle\overline{\boldsymbol{J}}\cdot\overline{\boldsymbol{B}}\rangle/\langle\overline{\boldsymbol{A}}\cdot\overline{\boldsymbol{B}}\rangle,\quad k_{\rm f}^2\equiv\langle\boldsymbol{j}\cdot\boldsymbol{b}\rangle/\langle\boldsymbol{a}\cdot\boldsymbol{b}\rangle. \tag{7}$$

For a fully helical field we also have $\langle\overline{\boldsymbol{J}}\cdot\overline{\boldsymbol{B}}\rangle=\pm k_{\rm m}\langle\overline{\boldsymbol{B}}^2\rangle$, $\langle\boldsymbol{j}\cdot\boldsymbol{b}\rangle=\mp k_{\rm f}\langle\boldsymbol{b}^2\rangle$, where the signs depend on the sign of the helicity. If the large and small small scale fields are not fully helical we have instead

$$\epsilon_{\rm m}\equiv\langle\overline{\boldsymbol{J}}\cdot\overline{\boldsymbol{B}}\rangle/(k_{\rm m}\langle\overline{\boldsymbol{B}}^2\rangle),\quad \epsilon_{\rm f}\equiv-\langle\boldsymbol{j}\cdot\boldsymbol{b}\rangle/(k_{\rm f}\langle\boldsymbol{b}^2\rangle), \tag{8}$$

where $\epsilon_{\rm m}$ and $\epsilon_{\rm f}$ quantify the fractions of the large and small scale fields that are helical. Inserting this into Eq. (6) yields

$$\langle\overline{\boldsymbol{B}}^2\rangle=\frac{\epsilon_{\rm f}k_{\rm f}}{\epsilon_{\rm m}k_{\rm m}}\langle\boldsymbol{b}^2\rangle, \tag{9}$$

which shows that the saturation amplitude of the mean field is proportional to the ratio of the scale separation, i.e. $k_{\rm f}/k_{\rm m}$, and that lowering the fractional helicity of the small scale field lowers the saturation amplitude of the large scale field. Moreover, lowering the fractional helicity of the large scale field actually enhances the saturation field strength.

All these aspects have been confirmed in Cartesian domains using numerical simulations; see Brandenburg & Subramanian (2005) for a review. Most surprising is perhaps the last aspect, i.e. that lowering the fractional helicity of the large scale field ($|\epsilon_{\rm m}|<1$) increases the saturation field strength. Simulations in a Cartesian box, where the boundaries in one direction are not periodic but perfectly conducting, show that the energy of the large scale magnetic field can exceed the kinetic energy (which is approximately the energy of the small scale field, denoted by $B_{\rm eq}^2$) by a factor that is equal to the scale separation ratio $k_{\rm f}/k_{\rm m}$ (Brandenburg 2001).

In the following we give a brief preliminary discussion of both helically forced simulations in spherical shell segments as well as mean field models in spherical shells.

3 Turbulence in spherical shell segments

Three dimensional turbulence simulations in spherical shell segments have been performed using an experimental version of the PENCIL CODE[1], which is a non-conservative, high-order, finite-difference code (sixth order in space and third order in time) for solving the compressible hydrodynamic equations.

In Fig. 1 we show a visualization of the three components of a snapshot of the magnetic field after it has reached

[1] `http://www.nordita.org/software/pencil-code`.

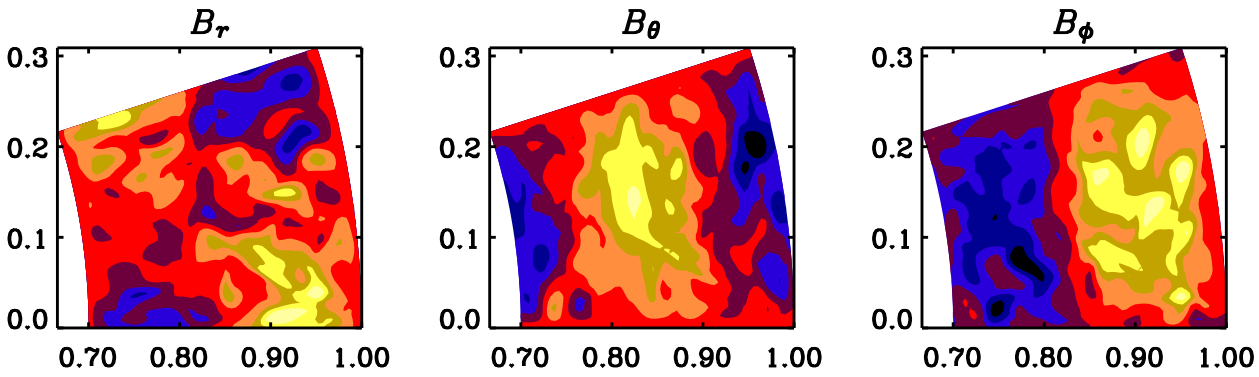

Fig. 1 Visualization of the three magnetic field components in an arbitrarily chosen meridional plane for a turbulent dynamo in a spherical segment with fully helical forcing with $R_{\rm m}=30$ (see text for boundary conditions).

saturation. In this run the magnetic Reynolds number is $R_{\rm m}=30$, where

$$R_{\rm m}=u_{\rm rms}/(\eta k_{\rm f}), \tag{10}$$

with $k_{\rm f}/k_{\rm m}=5$, and $k_{\rm m}=k_1$ with

$$k_1=2\pi/(R-R_{\rm in}) \tag{11}$$

where $R-R_{\rm in}$ is the the thickness of the shell whose inner and outer radii are given by R and $R_{\rm in}$. In the simulations presented here we have used $R_{\rm in}=0.7\,R$, which gives $k_1=21$ and $k_{\rm f}=105$. The latitudinal and longitudinal extent of the domain is $\pi/10$, so the domain is roughly cubical. This run uses periodic boundary condition along the azimuthal direction and perfectly conducting boundary conditions along the other two.

The azimuthal component, B_ϕ, is particularly prominent and shows a segregation of large scale positive and negative components in the radial direction, and a pattern in the latitudinal component that is shifted in the radial direction by 1/4 of the thickness of the shell.

The temporal evolution of the magnetic field is shown in Fig. 2. The energy of the total magnetic field exceeds the kinetic energy by about a factor of 3, most of which is contained in the mean field. These results are similar to behaviours observed in simulations in periodic Cartesian domains (see Brandenburg 2001).

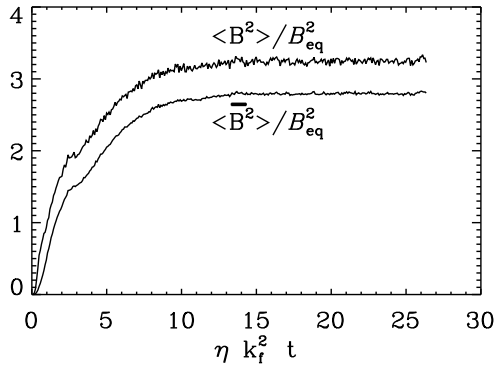

Fig. 2 Saturation behaviour of the normalized magnetic energies of the total field, $\langle\boldsymbol{B}^2\rangle$, and the mean field, $\langle\overline{\boldsymbol{B}}^2\rangle$, in a three-dimensional turbulence simulation with $R_{\rm m}=30$, i.e. the same run as in Fig. 1.

4 Mean field models

We next consider 2-dimensional axisymmetric simulations of Eq. (1) in spherical shells, but with a dynamical α effect that obeys its own time-dependent differential equation,

$$\frac{\partial\alpha}{\partial t}=-2\eta_{\rm t}k_{\rm f}^2\left(\frac{\alpha\overline{\boldsymbol{B}}^2-\eta_{\rm t}^2\overline{\boldsymbol{J}}\cdot\overline{\boldsymbol{B}}}{B_{\rm eq}^2}+\frac{\alpha-\alpha_{\rm K}}{R_{\rm m}}\right). \tag{12}$$

(Kleeorin et al. 1995, Blackman & Brandenburg (2002). The mean field models were computed using a modified version of the finite-difference code described in Käpylä et al. (2006). Note that α is now no longer constant, but it is quenched locally relative to the kinematic value, $\alpha_{\rm K}$, which is still spatially constant. In closed domains, such as those considered in this paper, the amount of quenching depends sensitively on the value of the magnetic Reynolds number, $R_{\rm m}\equiv\eta_{\rm t}/\eta$. Note also that there are no additional free parameters emerging from this type of nonlinearity.

We begin by considering first the saturation behaviour of the magnetic field in such a model. Figure 3 shows the evolution of $\langle\overline{\boldsymbol{B}}^2\rangle/B_{\rm eq}^2$ for a model with $R_{\rm m}=1000$, $k_{\rm f}R=100$, and $R_{\rm in}=0.5\,R$, as well as a case with $R_{\rm m}=30$ and $R_{\rm in}=0.7\,R$ (inset). Also shown is the fit

$$\frac{\langle\overline{\boldsymbol{B}}^2\rangle}{B_{\rm eq}^2}=\frac{\epsilon_{\rm f}k_{\rm f}}{\epsilon_{\rm m}k_{\rm m}}\left[1-e^{-2\eta k_{1,\rm eff}^2(t-t_{\rm sat})}\right], \tag{13}$$

where $t_{\rm sat}$ is approximately the time when the small scale field has saturated, and $k_{1,\rm eff}$ is a new effective wavenumber that might be related to that defined in Eq. (3), or even k_1

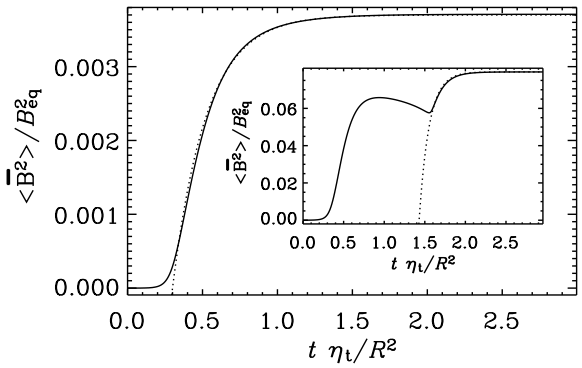

Fig. 3 Saturation behaviour of a mean field model with perfect conductor boundary condition for $R_{\rm m} = 1000$, $k_{\rm f}R = 100$, and $R_{\rm in} = 0.5\,R$. The inset shows the result for $R_{\rm m} = 30$ and $R_{\rm in} = 0.7\,R$. Dashed lines give the fit (13).

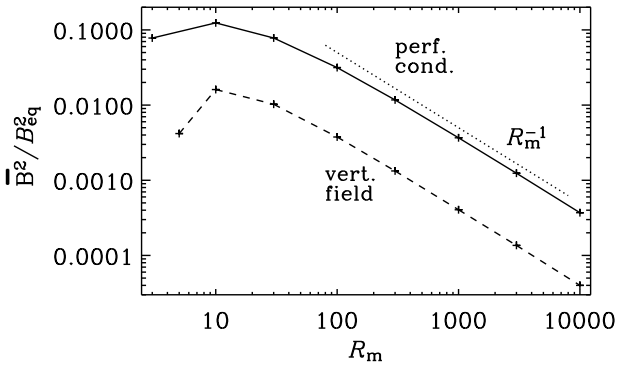

Fig. 4 Comparison of the saturation behaviours of a mean field model for perfect conductor (solid line) and vertical field (broken) boundary conditions.

defined in Eq. (11), but otherwise this is just treated as a fit parameter. For details regarding the derivation of this fit formula see Brandenburg (2001).

It turns out that, as the value of $R_{\rm m}$ is increased, the final saturation field strength of the large scale field decreases; see Fig. 4. This behaviour is familiar in the case of open boundary conditions, but it is unexpected in the case of perfectly conducting boundaries. The only difference between these two cases is that the energy is larger by a factor of about 10 when the boundaries are perfectly conducting.

Also depicted in Fig. 5 are the time traces of $\langle \overline{\boldsymbol{B}}^2 \rangle / B_{\rm eq}^2$ for different values of $R_{\rm m}$. Note that for models with $R_{\rm m} > 300$ there is a tendency for a decline of $\langle \overline{\boldsymbol{B}}^2 \rangle$ after having reached an initial maximum.

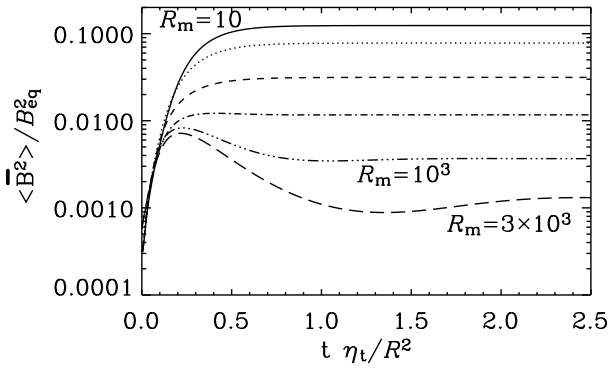

Fig. 5 Saturation behaviour of a mean field model with perfect conductor boundary condition with different values of $R_{\rm m}$, $k_{\rm f}R = 300$, and $R_{\rm in} = 0.5\,R$.

5 Conclusions

We have briefly presented preliminary results comparing direct simulations in spherical shell segments with their Cartesian analogues, on the one hand, and mean field models in spherical shells, on the other.

Simulations in Cartesian boxes and spherical shell segments both show qualitatively similar features in the mean magnetic field as well as similar saturation behaviour in the normalized mean magnetic field. On the other hand the saturation value is lower in mean field models than in the three-dimensional simulations.

Clearly more work is needed to clarify further the relation between these models, before we can proceed to the arguably more realistic case with a penetrable boundary. Work is in progress in this direction and will be reported elsewhere.

Acknowledgements. PJK acknowledges support from the Helsingin Sanomat foundation. DM is supported by Leverhulme trust. Computational resources were granted by CSC (Espoo, Finland) and QMUL HPC facilities purchased under the SRIF initiative.

References

Blackman, E. G., Brandenburg, A.: 2002, ApJ 579, 359
Brandenburg, A.: 2001, ApJ 550, 824
Brandenburg, A.: 2005, ApJ 625, 539
Brandenburg, A., Käpylä, P. J.: 2007, New J. Phys. 9, 305, 1
Brandenburg, A., Subramanian, K.: 2005, AN 326, 400
Browning, M. K., Miesch, M. S., Brun, A. S., Toomre, J.: 2006, ApJ 648, L157
Brun, A. S., Miesch, M. S. Toomre, J.: 2004, ApJ 614, 1073
Démoulin, P., Mandrini, C. H., van Driel-Gesztelyi, L., Thompson, B. J., Plunkett, S., Kovári, Z., Aulanier, G., Young, A.: 2002, ApJ 382, 650
Dikpati, M., Charbonneau, P.: 1999, ApJ 518, 508
Käpylä, P. J., Korpi, M. J., Tuominen, I.: 2006, AN 327, 884
Kleeorin, N., Rogachevskii, I., & Ruzmaikin, A.: 1995, A&A 297, 159

Krause, F., Rädler, K.-H.: 1980, *Mean-field magnetohydrodynamics and dynamo theory* (Pergamon Press, Oxford)
Moss, D., Tuominen, I., Brandenburg, A.: 1990, A&A 240, 142
Rogachevskii, I., Kleeorin, N.: 2003, PhRvE 68, 036301
Yousef, T. A., Brandenburg, A., Rüdiger, G.: 2003, A&A 411, 321